Synaptic mechanisms underlying interaural level difference selectivity in rat auditory cortex

Michael Kyweriga, Whitney Stewart, Carolyn Cahill and Michael Wehr

J Neurophysiol 112:2561-2571, 2014. First published 3 September 2014; doi:10.1152/jn.00389.2014

Journal of Neurophysiology publishes original articles on the function of the nervous system. It is published 12 times a year (monthly) by the American Physiological Society, 9650 Rockville Pike, Bethesda MD 20814-3991. ISSN: 0022-3077, ESSN: 1522-1598. Visit our website at http://www.the-aps.org/.

J Neurophysiol 112: 2561–2571, 2014.
First published September 3, 2014; doi:10.1152/jn.00389.2014.

Synaptic mechanisms underlying interaural level difference selectivity in rat auditory cortex

Michael Kyweriga,[1,2] Whitney Stewart,[1,3] Carolyn Cahill,[1] and Michael Wehr[1,4]

[1]*Institute of Neuroscience, University of Oregon, Eugene, Oregon;* [2]*Department of Biology, University of Oregon, Eugene, Oregon;* [3]*Department of Human Physiology, University of Oregon, Eugene, Oregon; and* [4]*Department of Psychology, University of Oregon, Eugene, Oregon*

Submitted 22 May 2014; accepted in final form 26 August 2014

Kyweriga M, Stewart W, Cahill C, Wehr M. Synaptic mechanisms underlying interaural level difference selectivity in rat auditory cortex. *J Neurophysiol* 112: 2561–2571, 2014. First published September 3, 2014; doi:10.1152/jn.00389.2014.—The interaural level difference (ILD) is a sound localization cue that is extensively processed in the auditory brain stem and midbrain and is also represented in the auditory cortex. Here, we asked whether neurons in the auditory cortex passively inherit their ILD tuning from subcortical sources or whether their spiking preferences were actively shaped by local inhibition. If inherited, the ILD selectivity of spiking output should match that of excitatory synaptic input. If shaped by local inhibition, by contrast, excitation should be more broadly tuned than spiking output with inhibition suppressing spiking for nonpreferred stimuli. To distinguish between these two processing strategies, we compared spiking responses with excitation and inhibition in the same neurons across a range of ILDs and average binaural sound levels. We found that cells preferring contralateral ILDs (often called EI cells) followed the inheritance strategy. In contrast, cells that were unresponsive to monaural sounds but responded predominantly to near-zero ILDs (PB cells) instead showed evidence of the local processing strategy. These PB cells received excitatory inputs that were similar to those received by the EI cells. However, contralateral monaural sounds and ILDs >0 dB elicited strong inhibition, quenching the spiking output. These results suggest that in the rat auditory cortex, EI cells do not utilize inhibition to shape ILD sensitivity, whereas PB cells do. We conclude that an auditory cortical circuit computes sensitivity for near-zero ILDs.

auditory cortex; interaural level difference; sound localization; synaptic inhibition; voltage-clamp

IN SENSORY CORTEX, synaptic interactions can transform neuronal response properties so that the tuning of the spiking output differs from that of the excitatory input. In this case, synaptic inhibition actively shapes the spiking output and shows different stimulus sensitivity than that of excitation. However, for many sensory features, the tuning of spiking responses is essentially the same as that of both the excitatory and the inhibitory input. We refer to this as "cotuning," in which the ratio of excitation and inhibition is proportional across the entire range of stimuli. In this case, inhibition does not have an active role in tuning; rather, the tuning of the neuron is inherited from the tuning of excitatory presynaptic neurons (or in some cases constructed by convergent excitatory input; as shown by Miller et al. 2001). Since the axonal projections from inhibitory interneurons are confined to local regions of the cortex (Markram et al. 2004; Thomson and Lamy 2007), an active role for inhibition indicates local synaptic processing. Distinguishing between these inheritance and local processing strategies requires the measurement of both the spiking responses and synaptic conductances within the same neurons. Using this approach in auditory cortex, recent work has shown that frequency tuning is largely inherited (Wehr and Zador 2003), whereas intensity tuning (Tan et al. 2007; Wu et al. 2006) and frequency-modulated sweep selectivity (Zhang et al. 2003) are both partly locally processed. However, little is known about whether or how cortical circuitry contributes to sound localization, a highly conserved auditory function that allows for the detection of unseen threats, prey, or conspecifics. Interaural level differences (ILDs) are key binaural sound localization cues for which many auditory cortical neurons are highly selective. The cortical processing strategies for ILD remain largely unknown.

Binaural interactions have been extensively studied with extracellular recordings in the auditory cortex of many different species such as the rat (Higgins et al. 2010; Kelly and Sally 1988), cat (Imig and Adrian 1977; Kitzes 2008; Phillips and Irvine 1983; Zhang et al. 2004), ferret (Campbell et al. 2006), pallid bat (Razak and Fuzessery 2010), and guinea pig (Rutkowski et al. 2000). However, unlike the visual system, in which binocularity first arises in the cortex, the same binaural selectivities seen in auditory cortex are also seen in the midbrain and are first computed in the LSO (Boudreau and Tsuchitani 1968). Whether cortical neurons inherit their ILD selectivity from subcortical neurons or whether cortical circuitry has an active role in binaural computations has remained mostly untested. Recent evidence from an intracellular study in cats (Ojima and Murakami 2002) and an extracellular study using a $GABA_A$ antagonist in the pallid bat suggests that the auditory cortex might actively process ILD cues (Razak and Fuzessery 2010). We therefore sought to examine directly the processing strategy of auditory cortical neurons for ILD sensitivity using in vivo whole cell recordings in the rat. We focused on two distinct classes of binaural selectivity: contralateral-preferring (EI) cells, which fire robustly to contralateral stimulation, and predominantly binaural (PB) cells, which fire robustly when both ears receive simultaneous sounds of equal levels (ILDs near 0) but not to monaural stimulation.

Here, we show the first direct evidence revealing how synaptic interactions construct spiking ILD selectivity in auditory cortical neurons. We found that EI cells received cotuned excitation and inhibition with excitation preceding inhibition by a few milliseconds for all binaural stimuli. ILD selectivity in these cells was not shaped by local inhibition, indicating an

Address for reprint requests and other correspondence: M. Wehr, 1254 Univ. of Oregon, Eugene, OR 97403-1254 (e-mail: wehr@uoregon.edu).

inheritance processing strategy. Similar to EI cells, PB cells received minimal synaptic input at ipsilateral ILDs and proportional excitation and inhibition for near-zero ILDs. However, for contralateral ILDs, PB cells received disproportionately strong synaptic inhibition, which even preceded excitation in some cells, quenching spiking output. This is evidence for the local processing strategy. Our results demonstrate that for a specific class of auditory cortical cells, PB cells, cortical synaptic inhibition plays an active role in shaping the spiking representation of sound localization cues.

METHODS

All procedures were in strict accordance with the National Institutes of Health *Guide for the Care and Use of Laboratory Animals* and approved by the University of Oregon Animal Care and Use Committee.

Physiology. We recorded from neurons in the left auditory cortex of 59 anesthetized (30 mg/kg ketamine, 0.24 mg/kg medetomidine) albino rats (*Rattus norvegicus*, Sprague-Dawley) aged 19–28 days postnatal (mean = 23.4 days, SD = 2.7). We used this age range to improve the yield of in vivo whole cell recordings (Kyweriga et al. 2014; Scholl et al. 2010). Rats older than 14–19 days, like adults, orient correctly toward sounds on the horizontal plane (Kelly et al. 1987). The critical period for hearing in rats is complete by approximately *postnatal day 14* (de Villers-Sidani et al. 2007), although some limited additional maturation of receptive fields and synaptic markers (e.g., NR1, GluR2, and GAD65) occurs until approximately *postnatal day 28* (Chang et al. 2005; Lu et al. 2008; Popescu and Polley 2010; Xu et al. 2007, 2010).

At the beginning of each experiment, we used multiunit recordings (1- to 2-MΩ tungsten microelectrodes; FHC) to map coarsely the auditory cortex. We sought to locate sites with robust binaural response properties. We targeted both primary auditory cortex (A1) and the suprarhinal auditory field (SRAF), which contains a relatively high proportion of PB cells (Higgins et al. 2010). We identified A1 from the caudal-rostral tonotopic gradient and a lack of responses on the dorsal border. We identified SRAF from the absence of auditory evoked responses along its ventral border (Higgins et al. 2010; Polley et al. 2007). We identified posterior auditory field (PAF) from the absence of auditory evoked responses along its posterior border and long latencies (Polley et al. 2007). We identified ventral auditory field (VAF) as the region between A1 and SRAF lacking responses on its posterior border (Polley et al. 2007).

Single-unit recordings. We obtained single-unit recordings with the loose cell-attached patch method, which provides excellent single-unit isolation. We only included cells in our sample if they fired at least one spike during the response window (between stimulus onset and 75 ms after stimulus offset) with a minimum of five trials per stimulus combination (n = 58 cells). Subpial depth for these cells ranged from 210 to 925 μm (mean = 561.0 μm, SD = 172.9) as determined from micromanipulator travel. Approximately 80% of these cells were located in A1 or SRAF with the remainder from either VAF or PAF.

Whole cell recordings. We used standard blind patch-clamp methods to obtain 58 whole cell recordings. We only included cells in our sample if they fired at least 1 spike during the response window (between stimulus onset and 75 ms after stimulus offset) with a minimum of 5 trials per stimulus combination (n = 58 cells). Subpial depth for these cells ranged from 187 to 857 μm (mean = 450.0 μm, SD = 167.1). Our whole cell recordings with both spiking and conductance data (28 cells) were located in either A1 (12 EI and 8 PB) or SRAF (3 EI and 5 PB). We did not use voltage-gated channel blockers in the pipette solution so that we could record both spiking output and synaptic currents from the same cells. The internal solution contained, in mM, 120 K-gluconate, 2 $MgCl_2$, 0.05 $CaCl_2$, 4 MgATP, 0.4 NaGTP, 10 Na_2-phosphocreatine, 13 BAPTA, and 10 HEPES, pH 7.28, diluted to 297 mosM, producing a calculated inhibitory reversal potential of −91.1 mV and an excitatory reversal potential of 3.4 mV. We corrected for a calculated liquid junction potential of 15.0 mV (Barry 1994) based on standard extracellular ionic concentrations (Sykova 1997), body temperature of 37°C, and dilution of our internal solution concentrations by ~10% (to achieve physiological osmolarity).

Many cells recorded in current-clamp did not spike at rest (I = 0 mode; Hromadka et al. 2008), but since many showed robust membrane potential depolarizations evoked by our stimulus array, we injected positive current to promote spiking in current-clamp mode (43–403 pA; mean = 147.6 pA, SD = 98.3; n = 20 cells).

In a subset of spiking cells, we also obtained voltage-clamp recordings to measure inhibitory and excitatory synaptic conductances. Holding potentials were stepped (with a 1-s ramp) to a pseudorandom sequence of 2 values using an Axopatch 200B amplifier. At each potential, after a 1-s equilibration period, 10 10-mV voltage pulses were delivered to monitor series and input resistance followed by acoustic stimuli. Across the voltage-clamp population, input resistance was 47.0 ± 25.8 MΩ, and series resistance was 40.1 ± 5.7 MΩ (median ± interquartile range, n = 28 cells). We measured synaptic currents at 2 holding potentials (mean = −110.6 mV, SD = 6.9, and mean = +27.6 mV, SD = 23.9; corrected for series resistance and liquid junction potential) and for 5–10 trials (median = 10) for each acoustic stimulus. Synaptic conductances, corrected for series resistance, were computed offline assuming an isopotential neuron (for details, see Wehr and Zador 2003). Deviations from this assumption can lead to underestimates of the magnitude of conductances. Thus all of our results are presented as relative measurements within cells and are normalized for group data analysis. To ensure high-quality voltage-clamp recordings, we only included cells with evoked conductances >0.5 nS for at least 5 stimulus combinations, resulting in a sample of 28 neurons. We found no significant physiological differences (independent samples t-test) between EI and PB cells for input resistance (P = 0.50), series resistance (P = 0.74), or recording depth (P = 0.37).

In summary, we recorded from 116 cells: 58 spiking cells with the cell-attached method and 58 spiking cells with the whole cell current-clamp method. Our whole cell data set contained 28 cells recorded in voltage-clamp mode.

Sound stimuli. Sound source localization depends on three cues: *1*) spectral cues due to the shape of the listener's head, pinnae, and hair; *2*) interaural time difference (ITD); and *3*) ILD. A recent study suggests that rats are unable to use ITD cues in sound localization tasks (Wesolek et al. 2010). We therefore used stimuli with ILD as the only sound localization cue. All stimuli were generated with custom software in MATLAB (MathWorks, Natick, MA) at a sampling rate of 192 kHz with a LynxTWO-B soundcard and delivered with Etymotic Research ER-2 earphones in sealed ear configuration. These earphones were suitable for our experiments as the rat audiogram is 7 octaves (0.5–64 kHz; Heffner et al. 1994; Kelly and Masterton 1977) and the ER-2 earphones cover over half of this range (4 octaves: 1–16 kHz). All experiments were performed in a double-walled sound isolation chamber with anechoic surface treatment. We sealed the ER-2 earphones along with Knowles omnidirectional electret condenser microphones into each ear.

The sound level inside each ear canal was then calibrated with the Knowles microphones, which were in turn calibrated with a Brüel & Kjær 4939 1/4-in. microphone before each experiment. To characterize binaural response properties, we used pseudorandomly interleaved Gaussian white noise bursts (25- or 100-ms duration) presented simultaneously to each ear from 10- to 50-dB sound-pressure level (SPL) in 10-dB steps (noise was not frozen between left and right or between each level). This produced an array of 25 binaural stimuli with a range of average binaural levels (ABLs; defined as the average

in decibels of the levels presented to the 2 ears) from 10 to 50 dB across a range of ILDs from −40 (ipsilateral) to +40 dB (contralateral); this range of ILDs probably exceeds the maximum physiological range of ILD in rats (Koka et al. 2008). Figure 1*A* shows this stimulus array with both coordinate systems included; ILD is on the *x*-axis and ABL is on the *y*-axis, whereas the levels in the ipsilateral ear and contralateral ear are on the diagonal axes (rotated by 45°). We also presented monaural sounds to each ear from 10 to 50 dB. These monaural responses are presented on each side of the binaural stimulus diamond (Fig. 1*A*) with ipsilateral sounds on the left and contralateral sounds on the right. This format is maintained throughout this report. We defined ipsilateral ILDs as negative and contralateral ILDs as positive. We restricted sound levels to a maximum of 50 dB because we noted that higher levels produced cross talk from one ear to the other, presumably due to sound transmission through the head (data not shown). All stimuli had 5-ms onset and offset ramps with 500-ms interstimulus intervals.

At the beginning of each experiment, we mapped auditory cortex with extracellular tungsten electrodes using pseudorandomly interleaved pure-tone pips (25-ms duration) to the contralateral ear. We presented tones in 1/4-octave steps from 1 to 16 kHz at 5 levels from 10 to 50 dB (SPL). All stimuli had 5-ms onset and offset ramps with 500-ms interstimulus intervals. Characteristic frequency was designated as the frequency that evoked responses at the lowest intensity. We were typically unable to measure the characteristic frequency of our whole cell recordings due to time constraints.

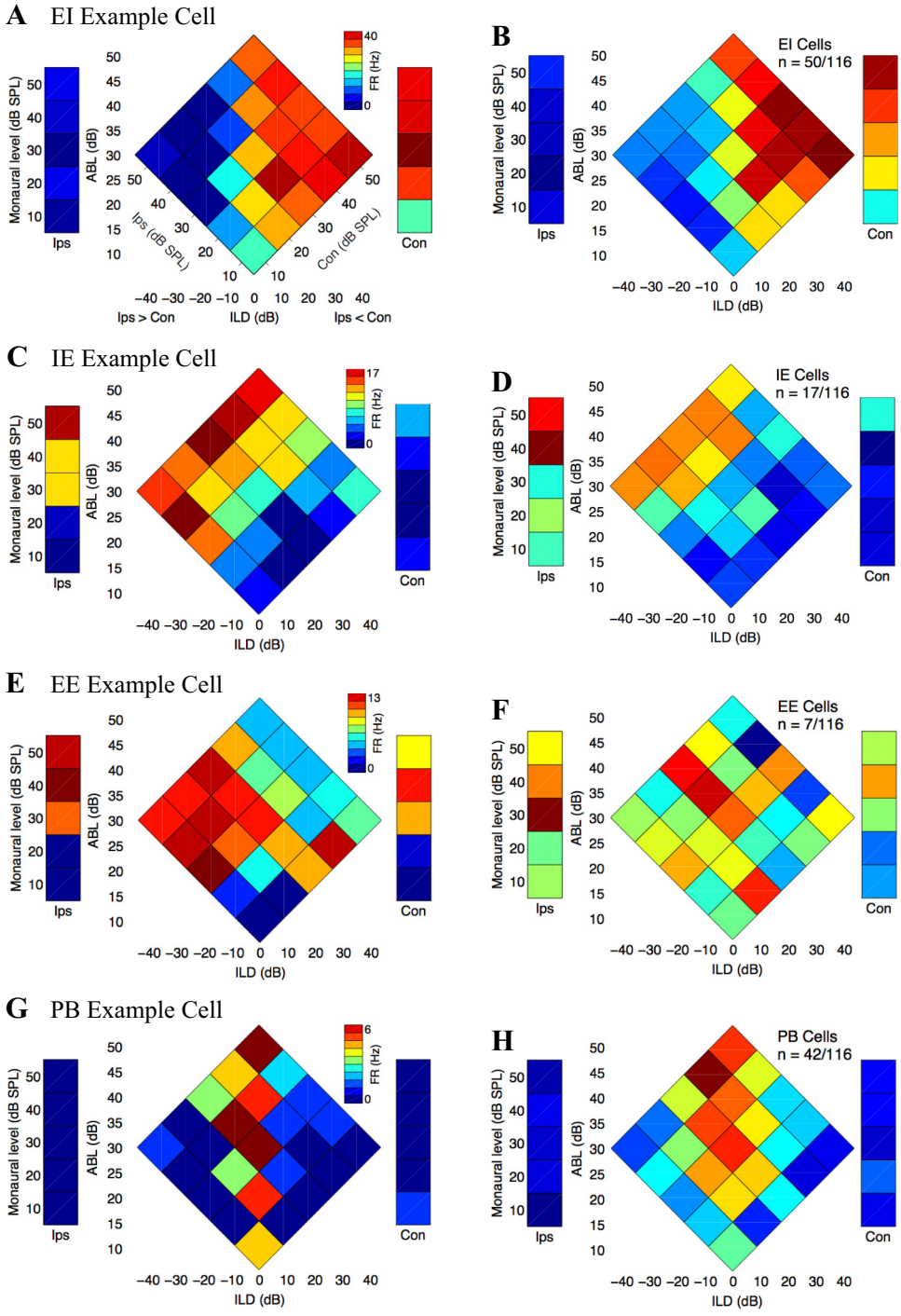

Fig. 1. Representative examples (*left* column) and group data (*right* column) of spiking responses comprising 4 binaural cell classes. *A*: an example of an EI cell (072710-WS-4) that responded to contralateral (Con) monaural and binaural sounds. The axes on the left side bar [ipsilateral (Ips)] show monaural sound levels from 10 to 50 dB (same scale for Con, right side bar). The axes on the central binaural plot show average binaural levels (ABLs) from 10 to 50 dB and interaural level differences (ILDs) from −40 dB (Ips > Con) to +40 dB (Con > Ips). These binaural sounds are composed of simultaneous monaural sounds denoted by the 45° rotated axes. These axes are consistent throughout this report. *B*: EI group data of normalized firing rate averaged across all cells. *C*: an example of an IE cell (080910-WS-3) that responded to ipsilateral monaural and binaural sounds. *D*: IE group data. *E*: an example of an EE example cell (080210-WS-1) that responded to monaural sounds from both ears and across all ILDs. *F*: EE group data. *G*: an example of a PB example cell (120810-MK-4) that was unresponsive to monaural sounds but responded strongly to ILDs from −10 to 0 dB. *H*: PB group data. Dark red indicates high firing rate, and dark blue indicates lack of response. FR, firing rate; SPL, sound-pressure level.

For whole cell recordings, we first recorded membrane potential responses to our stimulus set in current-clamp mode. Then we switched to voltage-clamp mode and measured the synaptic currents evoked by the same stimuli. Because of time constraints, we were often unable to record a voltage-clamp protocol with more than five trials for each holding potential, hence the reduced sample size ($n = 28$).

Classification of cells. To investigate the role of excitation and inhibition in cortical neurons responding to binaural stimuli, we first classified the spiking output of cells according to the monaural and binaural response categories presented by Zhang and colleagues (2004; see their Fig. 1) and then investigated the role of synaptic excitation and inhibition. Cells for which monaural sounds elicited firing rates three times above baseline firing rate for at least two sound levels were designated as "E," otherwise as "O," for each ear. By convention, we listed the contralateral ear first followed by the ipsilateral ear. Since the majority of our EO and OE cells were inhibited by the nondominant ear (the O ear) during binaural stimulation, we termed these cells EI and IE. For example, a cell responding only to contralateral monaural sounds and inhibited by the ipsilateral ear during binaural stimulation was designated EI. If a cell was unresponsive to monaural sounds in either ear (OO) but responded significantly to at least five binaural sounds, it was classified as PB. Cells failing to meet these criteria were considered unresponsive and were excluded from further analysis. Although responsive cells likely exist on a continuum instead of discrete categories (Campbell et al. 2006), here we grouped our cells into four categories to test specifically whether these groups have distinct synaptic processing strategies. Thus cells could be classified as EI (preferring contralateral sounds), IE (preferring ipsilateral sounds), EE (preferring both contralateral and ipsilateral sounds), or PB (unresponsive to monaural but responding predominantly to binaural sounds). In our sample of whole cell recordings with both spiking and conductances, we only observed two cell types: the EI and PB groups.

Data analysis. To extract spikes, we first high-pass filtered extracellular and intracellular recorded voltages at 300 Hz (Butterworth filter) and used an absolute threshold of 1–5 mV (median = 5 mV, mean = 3.8 mV, SD = 1.8). We quantified spiking responses by counting spikes in a 100-ms window (for 25-ms stimuli) or a 175-ms window (for 100-ms stimuli) following sound stimulus onset. We determine baseline firing rate from the time-averaged firing rate across the entire recording session (from sound onset of the 1st sound presented to 500 ms following the final stimulus).

To compute the ratio of excitatory to inhibitory synaptic conductances, we divided the peak of excitation by the sum of the peaks of excitation and inhibition. This produces a set of ratios that ranges from 0 (no excitation) to 1 (no inhibition) with 0.5 corresponding to equal peak conductances. To minimize the effects of potential errors in the estimation of absolute excitatory and inhibitory conductance amplitudes, we compared relative conductances within each cell. To perform ratio group analysis across cells, we first calculated the ratio for all stimulus combinations and then subtracted the lowest ratio from all stimulus combinations. We then divided all of these by the highest ratio. This produced a range of ratios in each cell between 0 and 1. Very small excitatory and inhibitory responses did not contribute to spiking, but very small values in the ratio denominator could lead to numerically unstable ratios. We therefore excluded stimulus combinations with conductances below 1 nS in the ratio analysis.

RESULTS

Neurons in auditory cortex are tuned to a range of ILDs. We classified auditory cortical neurons into four categories (EE, EI, IE, or PB) based on their spiking responses to monaural and binaural ILD stimuli (Fuzessery et al. 1990; Zhang et al. 2004). Here, E denotes monaurally responsive, and I denotes suppression by the nondominant ear with the contralateral ear listed first. For example, an EI cell is responsive to monaural contralateral sounds but not monaural ipsilateral sounds. Figure 1 shows examples and group data for each of these four cell types.

Figure 1*A* shows a representative example of an EI cell. This cell responded robustly to contralateral monaural sounds (vertical bar on right side) but not to ipsilateral monaural sounds (vertical bar on left side). Binaural stimuli elicited strong responses to ILDs from 0 to +40 dB but not to ILDs from −40 to −10 dB. Note that we defined contralateral ILDs as positive. The response profile of this EI cell was typical of all of our EI cells (Fig. 1*B*; $n = 50$ cells), which comprised 43.1% of our sample.

Figure 1*C* shows a representative example of an IE cell. This cell responded robustly to ipsilateral monaural sounds but not to contralateral monaural sounds. Binaural stimuli elicited strong responses to ILDs from −40 to +10 dB but not to ILDs from +20 to +40 dB. This response profile was typical of IE cells (Fig. 1*D*; −40 to 0 dB; $n = 17$ cells), which comprised only 14.7% of our spiking sample. We did not obtain any whole cell recordings from IE cells.

Figure 1*E* shows a representative example of an EE cell. This cell responded robustly to both contralateral and ipsilateral monaural sounds and across all ILDs. This response profile was typical of all EE cells (Fig. 1*F*; $n = 7$ cells), which were quite rare and comprised only 6% of our spiking sample. We did not obtain any whole cell recordings from EE cells.

Figure 1*G* shows a representative example of a PB cell. This cell was unresponsive to monaural sounds. However, this cell responded robustly to ILDs from −10 to 0 dB, which was typical of PB cells (Fig. 1*H*; $n = 42$ cells). PB cells comprised 36.2% of our spiking sample.

Contralateral-preferring (EI) cells inherit binaural response properties. We found that EI cells in rat auditory cortex inherited their binaural response properties. Figure 2 shows a representative example of an EI cell. The top traces in Fig. 2*A* show membrane potential responses at five ILDs from −40 to +40 dB at an ABL of 30 dB. This cell spiked robustly to contralateral stimulation at ILDs from 0 to +40 dB. After we recorded membrane potential responses in current-clamp mode, we switched to voltage-clamp and recorded excitatory and inhibitory currents and computed the synaptic conductances (bottom traces). Synaptic excitation had the same ILD sensitivity as spiking output, and inhibition was proportional to excitation. Figure 2*B* shows that this relationship remained consistent throughout all sound combinations in the full array of monaural and binaural sounds. Note that Fig. 2*A* is an excerpt from Fig. 2*B* (purple panels, center row). This cell responded robustly to monaural contralateral sounds and ILDs greater than −10 dB.

We next determined how excitatory-inhibitory interactions contributed to spiking output in the same neuron. To do this, we asked how firing rate depended on excitation and inhibition using linear regression analysis (Fig. 2, *C–E*). Firing rate strongly depended on excitatory conductance (Fig. 2*C*; $r^2 = 0.69$, $P = 3.8 \times 10^{-10}$; $n = 35$ stimulus combinations). Firing rate also depended significantly on inhibitory conductance (Fig. 2*D*; $r^2 = 0.68$, $P = 6.4 \times 10^{-10}$; $n = 35$ stimulus combinations), which may seem surprising at first because inhibition usually suppresses rather than increases spiking

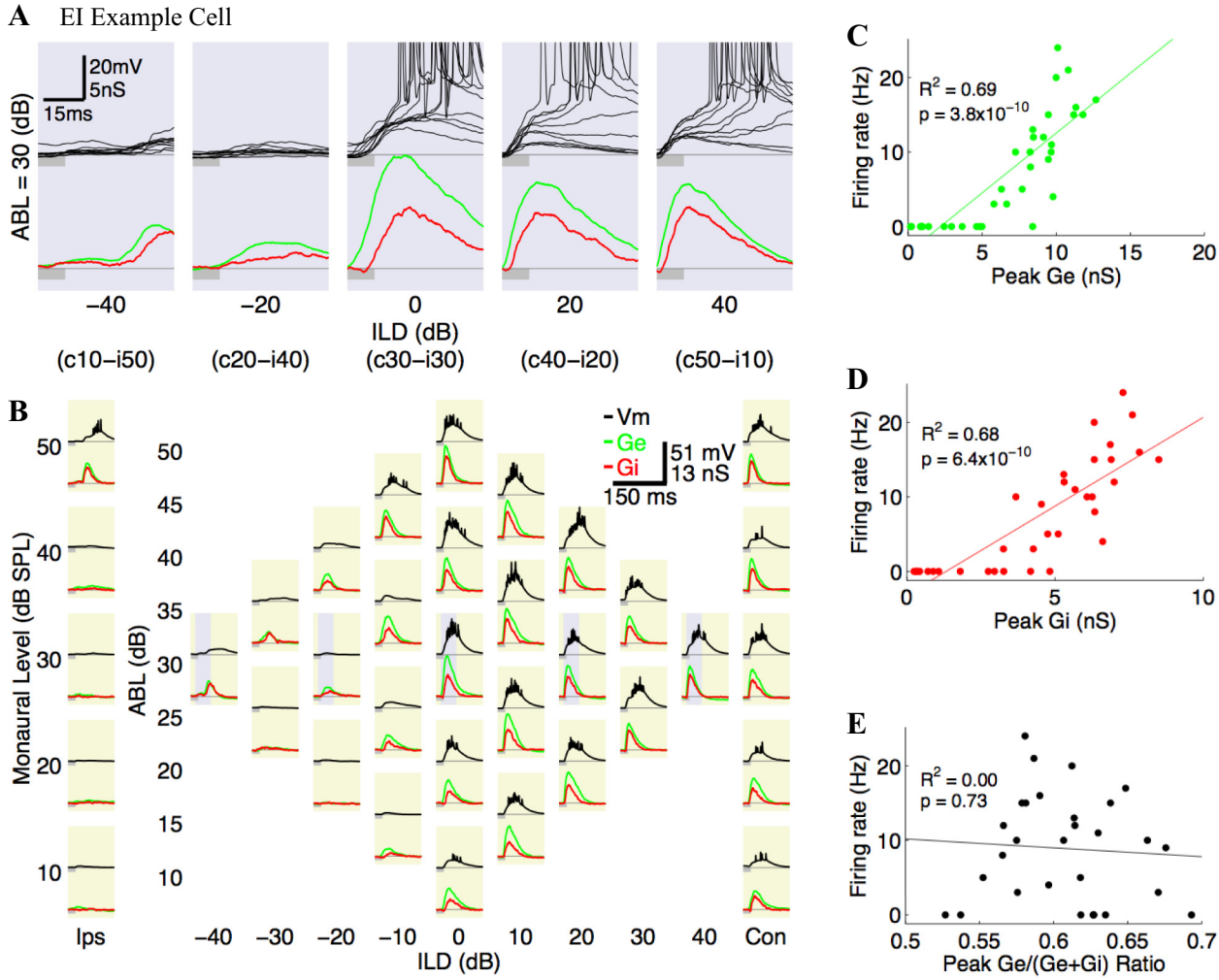

Fig. 2. Representative example of a contralateral-preferring (EI) cell (120810-MK-3) showing inheritance. *A*: top traces (black) show membrane potential at 5 ILDs with strong spiking responses from 0 to +40 dB (n = 10 trials for each ILD; spikes are truncated). Resting membrane potential is indicated by thin gray line (−67.7 mV). Bottom traces show excitation (Ge: green) and inhibition (Gi: red). Stimulus: 25-ms white noise burst (gray bars). Note that the beginning of the stimulus is truncated (time scale is 15–65 ms after stimulus onset to highlight timing differences between Ge and Gi). Sound level in each ear is indicated below each panel (c: contralateral; i: ipsilateral). *B*: complete binaural and monaural response map. Monaural sounds are columns on each side with Ips on the left and Con on the right. The binaural stimulus map is the middle diamond. Note that *A* is an excerpt from *B* (purple panels). *C–E*: regressions showing relationship between firing rate and conductance measures. Increases in excitation (*C*) and inhibition (*D*) strongly predicted increased firing rate. The ratio of excitation to inhibition (*E*) did not predict firing. In *E*, 6/35 stimulus combinations with excitation and inhibition <1 nS were excluded (see METHODS). Vm, membrane potential.

output. However, excitation was tightly correlated with inhibition (r = 0.96, $P = 1.4 \times 10^{-20}$; n = 35 stimulus combinations), indicating cotuning of excitation and inhibition, as has been previously reported (Wehr and Zador 2003). Indeed, firing rate was not significantly correlated with inhibition after controlling for the effect of excitatory conductance (partial correlation = 0.17, P = 0.32). Furthermore, spiking did not depend on the ratio of excitation to inhibition (Fig. 2*E*; r^2 = 0.0, P = 0.73). The relative timing of excitation to inhibition can affect spiking output. For example, inhibition typically lags behind excitation by a few milliseconds (Wehr and Zador 2003), but in some cases the timing of inhibition can reduce firing rates when it becomes coincident or precedes excitation (Higley and Contreras 2006). For this EI cell, the relative timing between excitation and inhibition did not affect spiking output since spiking showed a negative dependence on inhibitory delay (r^2 = 0.23, $P = 8.8 \times 10^{-3}$; n = 29/35 stimulus combinations). In this cell, inhibition lagged behind excitation across all stimulus combinations with a mean delay of 3.5 ms (SD = 2.9). These results indicate that the ILD sensitivity of the spiking output was inherited from that of the excitatory input and that the cotuned inhibition did not actively shape the ILD sensitivity of the cell.

Figure 3 shows spiking and conductance data for all 15 EI cells. Figure 3*A* shows the population spiking responses of EI cells after normalizing to their peak firing rates and averaging. These cells spiked to contralateral monaural sounds and to ILDs from 0 to +40 dB. Synaptic excitation and inhibition showed the identical pattern. On average, EI cells received strong excitation to monaural sounds and to ILDs from 0 to +40 dB (Fig. 3*B*). Similarly, these cells received strong inhibition to monaural sounds and to ILDs from 0 to +40 dB (Fig. 3*C*). As in the example cell above (Fig. 2), excitation and inhibition closely matched the spiking output of EI cells. To demonstrate this, we calculated the ratio of peak excitation to the sum of peak excitation and peak inhibition, normal-

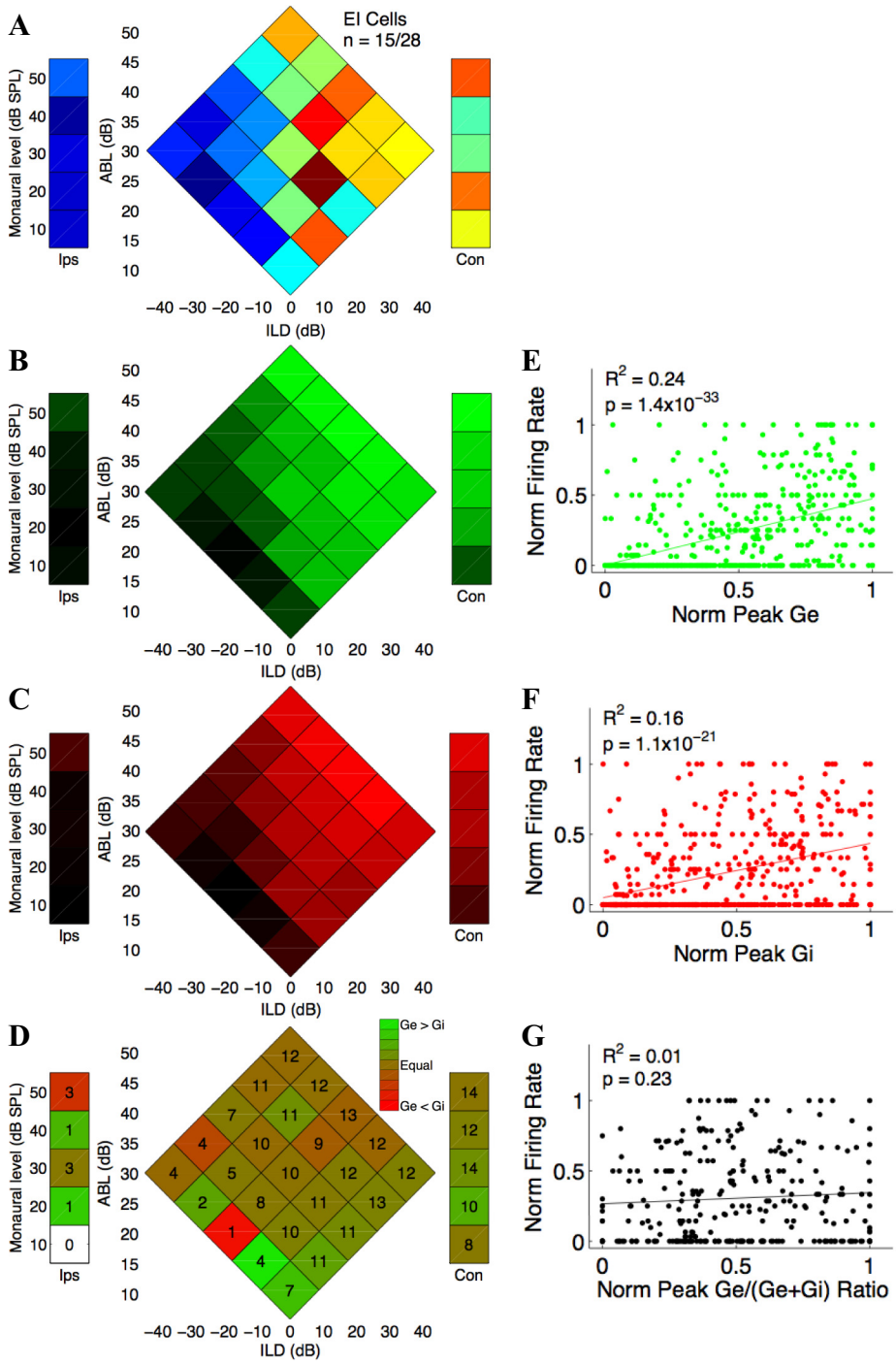

Fig. 3. Whole cell group data showing that EI cells inherit their spiking response profiles (n = 15 cells). *A*: averaged normalized firing rate. Maximal responses are red, and minimal responses are blue. *B*: averaged normalized peak excitatory conductances. *C*: averaged normalized peak inhibitory conductances. In *B* and *C*, maximal conductances are colored, and minimal conductances are black. *D*: averaged normalized ratio of excitation to inhibition. Number of cells included are overlaid on each stimulus combination. Note that the few unbalanced ratios (bright red or green) are due to increased variance from small sample size. *E–G*: linear regression analysis between firing rate and conductance measures. Firing rate was strongly dependent on peak excitation (*E*) and peak inhibition (*F*) but independent of the ratio of excitation to inhibition (*G*).

ized to the range 0 to 1 for each cell. Across the population (Fig. 3*D*), this ratio was essentially equal across all stimulus combinations.

To assess directly how firing rate depended on excitation and inhibition, we again used linear regression analysis. Figure 3, *E–G*, shows, for all EI cells, the same linear regressions as shown for the example cell above (Fig. 2, *C–E*). Across the population, spiking output significantly depended on synaptic excitation (Fig. 3*E*; $r^2 = 0.24$, $P = 1.4 \times 10^{-33}$). Because of cotuning, spiking output also depended on inhibition (Fig. 3*F*; $r^2 = 0.16$, $P = 1.1 \times 10^{-21}$), and excitation and inhibition were tightly correlated ($r = 0.74$, $P = 6.1 \times 10^{-94}$). Thus after accounting for excitation, inhibition was no longer predictive of firing (partial correlation = 0.06, $P = 0.16$). The spiking of EI cells was independent of the ratio of peak excitation to the sum peak of excitation and inhibition (Fig. 3*G*; $r^2 = 0.01$, $P = 0.23$). Last, we found a weak and negative dependence on the relative timing between excitation and inhibition ($r^2 = 0.02$, $P = 0.03$). We conclude that the ratio and relative timing of excitation and inhibition did not have a role in shaping the spiking ILD selectivity of EI cells.

These results taken together suggest that the monaural and binaural ILD sensitivity of EI cells is inherited. The spiking output of EI cells depended simply on the total magnitude of

synaptic conductance. For nonpreferred ILDs and monaural sounds, EI cells did not fire simply because they received little or no synaptic input.

PB cells exhibit synaptic computation of binaural response properties. PB cells showed a strikingly different pattern of synaptic input than EI cells. Rather than the inheritance strategy, PB cells displayed evidence of the local processing strategy. Figure 4 shows a representative example of a PB cell. The top traces (Fig. 4*A*) show membrane potential responses at five ILDs from −40 to +40 dB. This cell spiked robustly only to a narrow range of ILDs from −20 to 0 dB. In contrast to EI cells, the balance of excitation and inhibition depended strongly on ILD. At −20-dB ILD, excitation and inhibition were approximately balanced, which drove robust spiking responses. However, at +20- and +40-dB ILD, inhibition far outweighed excitation, and the cell fired no spikes. The full binaural array in Fig. 4*B* shows that spiking in this cell was unresponsive to monaural stimuli but was robust for ILDs of −30 to +10 dB (top traces). The imbalance of inhibition at contralateral ILDs is apparent in the bottom red and green traces. For ipsilateral monaural sounds and ILDs of −40 to −10 dB, peak excitation and inhibition were roughly equal. However, for contralateral ILDs (0 to +40 dB), there was both a withdrawal of excitation and very strong inhibition that together prevented spiking output.

To quantify how these synaptic interactions shaped spiking output, we asked how firing rate depended on excitation and inhibition using linear regression analysis (Fig. 4, *C–E*). Firing rate strongly depended on excitatory conductance (Fig. 4*C*; $r^2 = 0.59$, $P = 4.6 \times 10^{-8}$; $n = 35$ stimulus combinations) but only weakly depended on inhibitory conductance (Fig. 4*D*; $r^2 = 0.14$, $P = 0.025$; $n = 35$ stimulus combinations). This makes sense because, unlike in EI cells, which showed cotuning of excitation and inhibition ($r = 0.96$ for the EI cell in Fig. 2), synaptic excitation and inhibition in this PB cell were less correlated ($r = 0.85$, $P = 3.3 \times 10^{-11}$). When we controlled for the effect of excitatory conductance, firing rate was strongly negatively correlated with inhibition (partial correlation: $r = -0.85$, $P = 7.6 \times 10^{-11}$). This lack of cotuning is a signature of the local processing strategy: as inhibition in-

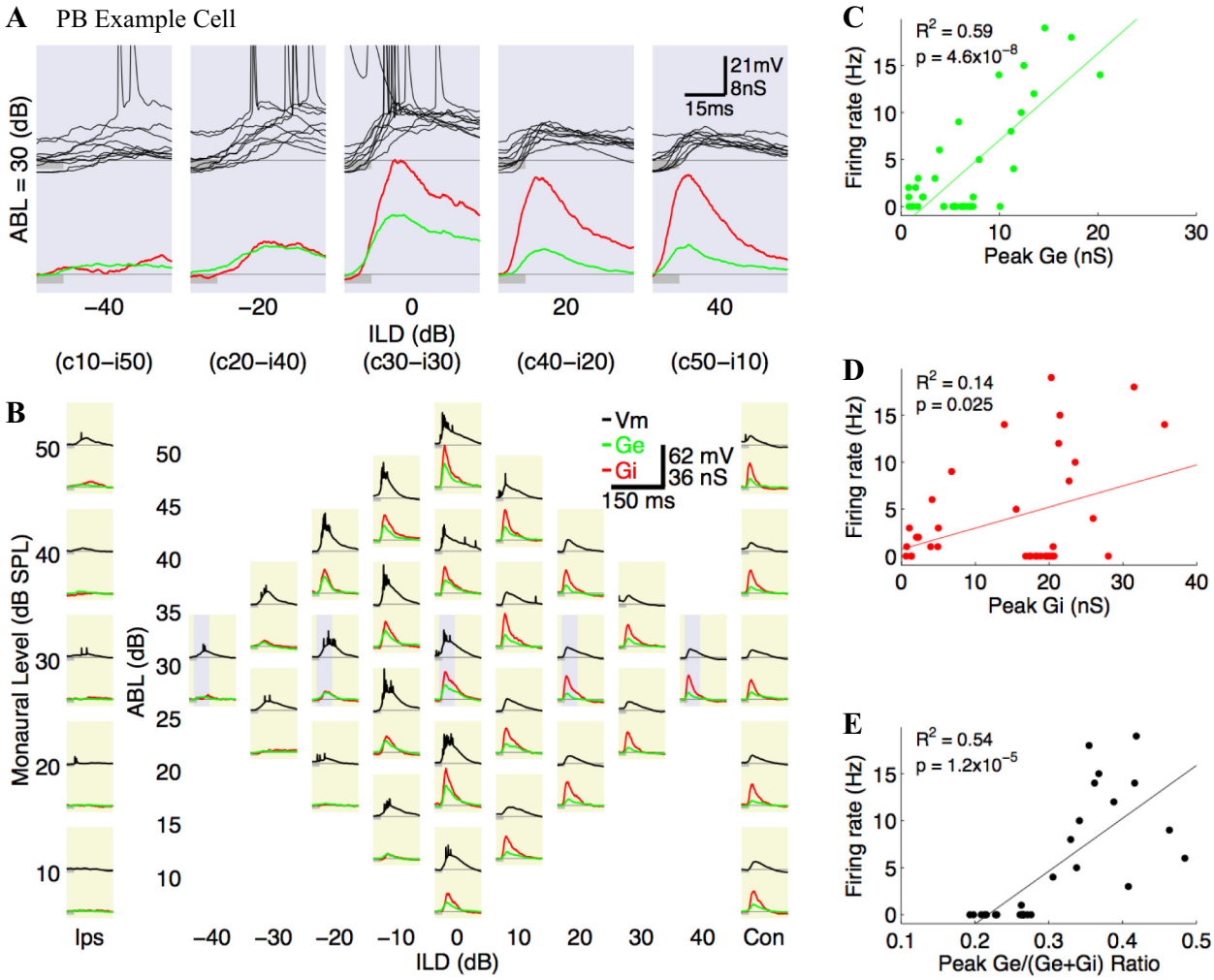

Fig. 4. Representative example of a predominantly binaural (PB) cell (120810-MK-5) showing the local processing strategy. *A*: top traces (black) show membrane potential at 5 ILDs (ABL = 30 dB) showing strong spiking responses to ILDs at −20- and 0-dB ILD (10 trials for each ILD; spikes are truncated). Resting membrane potential is indicated by thin gray line (−61.8 mV). Bottom traces show excitation (Ge: green) and inhibition (Gi: red). Format is as in Fig. 2. *B*: complete binaural and monaural response map. Note that *A* is an excerpt from *B* (purple panels). *C–E*: regressions showing relationship between firing rate and conductance measures. Excitation strongly predicted the firing rate (*C*), but inhibition only weakly (*D*). The ratio of excitation to inhibition (*E*) predicted firing rate. In *E*, 8/35 stimulus combinations with peak excitation and peak inhibition <2 nS were excluded.

creased, spiking decreased. Accordingly, spiking was dependent on the ratio of excitation to inhibition (Fig. 4*E*; $r^2 = 0.54$, $P = 1.2 \times 10^{-5}$), unlike EI cells. In this cell, the relative timing between excitation and inhibition weakly affected spiking output ($r^2 = 0.22$, $P = 0.01$; $n = 27/35$ stimulus combinations). As the inhibitory lag decreased, so, too, did the firing rate. For this cell, inhibition lagged behind excitation at negative ILDs (see Fig. 4*A* at ILDs of −40 and −20 dB) but preceded excitation at positive ILDs (see Fig. 4*A* at ILDs of +20 and +40 dB), adding to inhibitory shaping of the spiking output of the cell. These results indicate that the spiking output of this PB cell were strongly shaped by excitatory-inhibitory interactions. At ipsilateral and central ILDs, the spiking response of this PB cell was driven by a volley of balanced excitation and inhibition. At contralateral ILDs, however, spiking was quenched by inhibition that was both more powerful than and preceded excitation.

Across the population (Fig. 5), PB cells were generally very similar to the example cell shown in Fig. 4. PB cells were unresponsive to monaural sounds and fired predominantly to ILDs near 0 dB (Fig. 5*A*). They received strong excitation at central ILDs from −20 to +20 dB and modest excitation at contralateral monaural sounds and ILDs at +30–40 dB. However, these cells received strong contralateral inhibition to

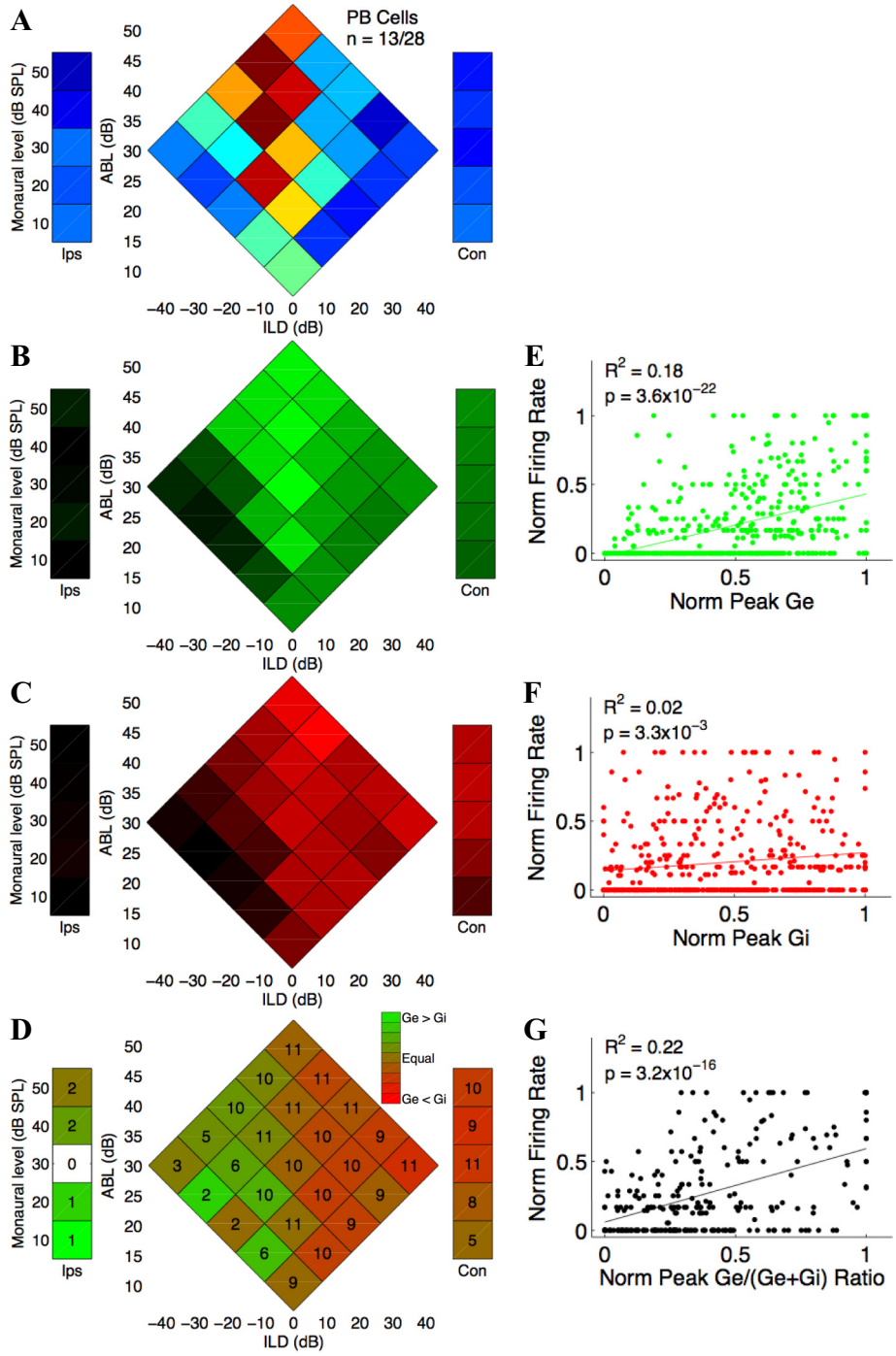

Fig. 5. Whole cell group data showing that the spiking of PB cells ($n = 13$) is controlled by excitatory-inhibitory interactions (local processing). *A*: averaged normalized firing rate. Maximal responses are red, and minimal responses are blue. *B*: averaged normalized peak excitatory conductances. *C*: averaged normalized peak inhibitory conductances. In *B* and *C*, maximal conductances are colored, and minimal conductances are black. *D*: averaged normalized ratio of excitation to inhibition. Number of cells included are overlaid on each stimulus combination. *E–G*: linear regression analyses between firing rate and conductance measures. Firing rate was strongly dependent on peak excitation (*E*) but more weakly dependent on inhibition (*F*). *G*: firing rate was strongly dependent on the ratio of excitation to inhibition.

monaural sounds and ILDs from −10 to +40 dB (Fig. 5*C*). As shown for the example PB cell (Fig. 4), inhibition far outweighed excitation at contralateral ILDs and monaural contralateral sounds across all PB cells. Excitatory input showed some weak selectivity for best ILD, indicating that the PB spiking response profiles were partially inherited. However, spiking at contralateral ILDs was suppressed by inhibitory drive that overpowered excitation (compare Fig. 5*A* with Fig. 5, *B* and *C*). To demonstrate further how these excitatory-inhibitory interactions drove spiking output, we again normalized the ratio of peak excitation to the sum of peak excitation and inhibition (as we did above for EI cells). Figure 5*D* shows that excitation and inhibition were not cotuned but rather that the relative contributions of excitation and inhibition varied systematically with ILD. The E-to-I ratio at ipsilateral ILDs from −40 to −10 dB showed more excitation; however, at contralateral monaural sounds and ILDs from 0 to +40 dB, inhibition was much stronger than excitation (compare Fig. 5*D* with Fig. 3*D*).

To assess directly how firing rate depended on excitation and inhibition, we again used linear regression. Figure 5, *E–G*, shows, for all PB cells, linear regressions of firing rate to synaptic input. As with the example PB cell shown in Fig. 3, spiking output significantly depended on synaptic excitation in all PB cells (Fig. 5*E*; $r^2 = 0.18$, $P = 3.6 \times 10^{-22}$). However, spiking output was only weakly dependent on inhibition (Fig. 5*F*; $r^2 = 0.02$, $P = 3.3 \times 10^{-3}$). This suggests that inhibition actively suppressed the spiking output of most PB cells. Similar to EI cells, excitation and inhibition were correlated ($r = 0.57$, $P = 5.9 \times 10^{-41}$), but when accounting for excitation, spiking output of PB cells was negatively correlated with inhibition (partial correlation = −0.14, $P = 2.1 \times 10^{-3}$). Accordingly, and in contrast with EI cells, the ratio of excitation and inhibition had a strong role in shaping the spiking output of PB cells (Fig. 5*G*; $r^2 = 0.22$, $P = 3.2 \times 10^{-16}$). In a subset of PB cells (3/13, e.g., Fig. 4), spiking showed a significant dependence on the timing of excitation to inhibition, but this was not true at the population level ($r^2 = 0.0$, $P = 0.33$).

Taken together, these results indicate that PB cells in auditory cortex show local synaptic processing of binaural ILD cues. At central ILDs, spiking output in these cells directly depended on the magnitude of synaptic conductances. In contrast, at contralateral ILDs, PB cells received strong excitation but did not spike due to even more powerful synaptic inhibition.

DISCUSSION

Here, we have demonstrated a novel role for inhibition in sensory cortex in the shaping of binaural sensitivity in predominantly binaural cells. These PB cells responded robustly when sound level was similar in each ear or somewhat favored the ipsilateral ear (ILDs around −20 to 0 dB). These cells were somewhat similar to contralateral-preferring (EI) cells in that ipsilateral sounds (monaural and ILDs from −40 to 0 dB) evoked excitation and inhibition that was proportional but usually too weak to evoke spiking output. Both of these cell classes began to spike at ILDs near 0 dB, once they received sufficient excitation. However, unlike EI cells, for contralateral sounds (monaural and ILDs >0 dB), PB cells received disproportionately stronger synaptic inhibition than excitation. This contralateral-evoked inhibition silenced spiking by reversing of the relative magnitudes of excitation and inhibition. In a few cases, there was also a reversal of the relative timing of synaptic inhibition (3/13 PB cells).

Neurons in sensory cortex typically show cotuning of excitation and inhibition for stimulus dimensions such as frequency in auditory cortex (Wehr and Zador 2003) and orientation in visual cortex (Tan et al. 2011). Cotuning of excitation and inhibition indicates that the tuning of spiking responses is not actively shaped by local inhibition but rather is inherited from the tuning of presynaptic excitatory neurons. The simplest scenario for this is that presynaptic neurons have ILD sensitivity similar to that of the excitatory input to cortical neurons. This is consistent with the existence of both EI and PB neurons in subcortical structures such as the inferior colliculus, where these binaural properties show local transformation (Fuzessery et al. 1990; Li et al. 2010). However, because our methods measured the summed excitatory input by the neuron, it is also possible that this excitation is pooled across a population of neurons with distinct ILD sensitivity. In the visual cortex, for example, orientation selectivity arises from pooled thalamic inputs that have aligned circularly symmetric receptive fields (Reid and Alonso 1995). Orientation tuning is further refined by local cortical inhibition (Hirsch and Martinez 2006), suggesting a similar principle of operation as seen in our PB cells, for which ILD sensitivity is partially inherited and is markedly refined by local cortical inhibition.

Estimation of excitatory and inhibitory conductances from somatic voltage-clamp is subject to errors arising from imperfect space clamp (Wehr and Zador 2003; Williams and Mitchell 2008). Because systematic errors apply to all responses of a cell, within-cell comparisons such as we have made here are relatively unsusceptible to such errors. Nevertheless, apparent shifts in the relative strength of synaptic excitation and inhibition could be produced if different stimuli activated distinct spatial distributions of synapses within the dendritic arbor. Two observations allay concern about this possibility. First, imaging of calcium transients in individual spines on auditory cortical neurons has revealed that the tuning of synapses is heterogeneous and interspersed (Chen et al. 2011), suggesting that systematic shifts in the spatial distribution of activated synapses for different stimuli is unlikely. Second, we note that even if a shift in the spatial distribution of distal synaptic input produced an apparent difference in the excitation and inhibition measured at the soma, this apparent effect is what is actually experienced by the soma and is therefore more relevant to spiking output than the actual synaptic conductances in the distal dendrites.

Role of inhibition in cortical ILD selectivity. PB cells received broadly tuned excitatory inputs ranging from ILDs near zero to very contralateral. At the more contralateral stimulus combinations, inhibition reduced or abolished spiking output because it overwhelmed excitation. In a few cases, this effect was enhanced by shifts in the relative timing of excitation and inhibition with inhibition preceding excitation for contralateral ILDs. An effect of the relative timing of inhibition has only been observed in a few cases in the cortex, such as FM sweep selectivity (Zhang et al. 2003), whisker directional selectivity (Wilent and Contreras 2005), and silencing of auditory layer VI cells (Zhou et al. 2010). Whereas only 3/13 PB cells in our

sample showed preceding inhibition that suppressed spiking, we never observed this in our EI sample (0/15 cells). Because of our small sample size, we cannot rule out the possibility that EI cells use this strategy, but our results suggest that the relative timing of excitation and inhibition may specifically contribute to PB but not EI response properties in auditory cortex. These results are an important first step toward understanding the role of cortical inhibitory interneurons in sound localization. The direct comparison between synaptic conductances and spiking output in the same cells is central to understanding cortical circuits (Isaacson and Scanziani 2011) but is still rare (Wehr and Zador 2003; Wu et al. 2011). With this approach, we have identified the computation of PB selectivity as an important role for cortical inhibition, but several questions remain about the neuronal sources of these inhibitory inputs. Which class or classes of inhibitory interneurons target PB cells? Do they receive the same or a different set of excitatory inputs than the PB cell they target? Does the contralaterally evoked inhibition that converts EI neurons into PB neurons arise from the same or a different set of inhibitory neurons than the centrally evoked inhibition? Further investigation using molecular-genetic methods for identification and manipulation of these neurons and circuits may help provide answers to these questions.

Comparison with previous studies. It is still not entirely clear whether binaural response properties in cortex fall into discrete classes, as has been widely proposed (e.g., Zhang et al. 2004), or fall along a continuum, as recent work suggests (Campbell et al. 2006). Our findings provide novel insight into this debate because we have shown that two distinct classes of binaural spiking responses, EI and PB, are produced by distinct synaptic processing strategies. However, it is important to note that because we targeted EI and PB neurons, our sample could be biased toward discrete categories, suggesting that the existence of a continuum should not be ruled out.

Two recent studies showed that cortical responses to binaural sounds in the rat are tuned to contralateral sources. Yao et al. (2013) reported that cells in rat primary auditory cortex are exclusively tuned to contralateral azimuths. Similarly, Chadderton and colleagues (2009) found panoramic synaptic representations of free-field sound sources with half of their sample spiking to contralateral sources and the remainder divided between center and ipsilateral locations. Many of our cells, especially EI cells, received synaptic inputs across all ILDs (see Fig. 2*B*). However, cells in our PB sample tended to receive contralateral but not ipsilateral synaptic input (see Fig. 4*B*). The discrepancy between our present work and that of Yao et al. (2013) could be due to differences between free-field and binaural stimuli. For free-field sounds, cortical cells may integrate information from both ILD and the head-related transfer function. Future studies in the rat are necessary to reveal the mechanisms underlying the integration of these two sound localization cues in the cortex.

In future studies, optogenetic silencing may provide a means to test directly the role of auditory cortex in sound localization without the long-term complications of conventional lesion studies. In the pallid bat, local inhibitory blockade in auditory cortex converts PB cells into EI cells, whereas EI cells remain unchanged (Razak and Fuzessery 2010). Our results are consistent with this finding, suggesting that cortical inhibition shapes the spiking output of PB cells. Here, by directly measuring the membrane potential and synaptic excitation and inhibition, we show that inhibition shapes spiking output of PB cells both by overpowering excitation in magnitude and, in some cases, by preceding excitation in time. These results suggest a role for the auditory cortex in processing binaural cues for sound localization. Moreover, our results demonstrate that cortical synaptic processing of binaural cues is not just a specialization in a nocturnal predator, suggesting that this auditory cortical circuit is a general feature of mammalian auditory systems.

Why is binaural selectivity computed at multiple levels of the auditory system? Binaural cues such as ILD undergo extensive synaptic processing in the auditory brain stem and midbrain (Li et al. 2010), and both EI and PB neurons are present in the inferior colliculus (Fuzessery et al. 1990; Irvine and Gago 1990). Why then should PB selectivity be recomputed in auditory cortex rather than simply inherited from subcortical PB neurons as with cortical EI neurons? One possibility is that there is a lack of precision in axonal projections from the thalamus into the cortex (Miller et al. 2001). This would require a recomputation of PB selectivity. However, this would not explain why only PB cells and not EI cells require active processing. Another interpretation of our finding is that it underscores the adaptive value of sound localization; some neural computations may be redundant precisely because they are critical to survival of a species over evolutionary time frames. However, cortical recomputation of binaural selectivity might serve a different purpose than subcortical binaural representations. We speculate that cortical synaptic control over binaural selectivity might provide a substrate for modulation by selective attention (Lee and Middlebrooks 2011). Thus PB cells, but not EI cells, would be well-suited for regulatory control of their binaural response properties by modulating the efficacy of synaptic inhibition. The mechanisms by which we can attend to a particular location in space are not well-understood, but online regulation of the binaural selectivity of cortical neurons by modulation of inhibitory circuitry is an interesting possibility.

ACKNOWLEDGMENTS

We thank Aldis Weible and Alexandra Moore for thoughtful discussions and the University of Oregon Animal Care Services for taking exceptional care of our laboratory animals.

GRANTS

This work was supported by National Institute of Deafness and Other Communications Disorders Grant 1R01-DC-011379, National Science Foundation Division of Biological Infrastructure Award BIO755581, the Post-9/11 Montgomery GI Bill, and the Whitehall Foundation.

DISCLOSURES

No conflicts of interest, financial or otherwise, are declared by the author(s).

AUTHOR CONTRIBUTIONS

M.K. and M.W. conception and design of research; M.K., W.S., and C.C. performed experiments; M.K. analyzed data; M.K. and M.W. interpreted results of experiments; M.K. prepared figures; M.K. drafted manuscript; M.K. and M.W. edited and revised manuscript; M.K. and M.W. approved final version of manuscript.

REFERENCES

Barry PH. JPCalc, a software package for calculating liquid junction potential corrections in patch-clamp, intracellular, epithelial and bilayer measurements and for correcting junction potential measurements. *J Neurosci Methods* 51: 107–116, 1994.

Boudreau JC, Tsuchitani C. Binaural interaction in the cat superior olive S segment. *J Neurophysiol* 31: 442–454, 1968.

Campbell RA, Schnupp JW, Shial A, King AJ. Binaural-level functions in ferret auditory cortex: evidence for a continuous distribution of response properties. *J Neurophysiol* 95: 3742–3755, 2006.

Chadderton P, Agapiou JP, McAlpine D, Margrie TW. The synaptic representation of sound source location in auditory cortex. *J Neurosci* 29: 14127–14135, 2009.

Chang EF, Bao SW, Imaizumi K, Schreiner CE, Merzenich MM. Development of spectral and temporal response selectivity in the auditory cortex. *Proc Natl Acad Sci USA* 102: 16460–16465, 2005.

Chen X, Leischner U, Rochefort NL, Nelken I, Konnerth A. Functional mapping of single spines in cortical neurons in vivo. *Nature* 475: 501–505, 2011.

de Villers-Sidani E, Chang EF, Bao SW, Merzenich MM. Critical period window for spectral tuning defined in the primary auditory cortex (A1) in the rat. *J Neurosci* 27: 180–189, 2007.

Fuzessery ZM, Wenstrup JJ, Pollak GD. Determinants of horizontal sound location selectivity of binaurally excited neurons in an isofrequency region of the mustache bat inferior colliculus. *J Neurophysiol* 63: 1128–1147, 1990.

Heffner HE, Heffner RS, Contos C, Ott T. Audiogram of the hooded Norway rat. *Hear Res* 73: 244–247, 1994.

Higgins NC, Storace DA, Escabi MA, Read HL. Specialization of binaural responses in ventral auditory cortices. *J Neurosci* 30: 14522–14532, 2010.

Higley MJ, Contreras D. Balanced excitation and inhibition determine spike timing during frequency adaptation. *J Neurosci* 26: 448–457, 2006.

Hirsch JA, Martinez LM. Circuits that build visual cortical receptive fields. *Trends Neurosci* 29: 30–39, 2006.

Hromadka T, Deweese MR, Zador AM. Sparse representation of sounds in the unanesthetized auditory cortex. *PLoS Biol* 6: e16, 2008.

Imig TJ, Adrian HO. Binaural columns in the primary field (A1) of cat auditory cortex. *Brain Res* 138: 241–257, 1977.

Irvine DR, Gago G. Binaural interaction in high-frequency neurons in inferior colliculus of the cat: effects of variations in sound pressure level on sensitivity to interaural intensity differences. *J Neurophysiol* 63: 570–591, 1990.

Isaacson JS, Scanziani M. How inhibition shapes cortical activity. *Neuron* 72: 231–243, 2011.

Kelly JB, Judge PW, Fraser IH. Development of the auditory orientation response in the albino rat (*Rattus norvegicus*). *J Comp Psychol* 101: 60–66, 1987.

Kelly JB, Masterton B. Auditory sensitivity of the albino rat. *J Comp Physiol Psychol* 91: 930–936, 1977.

Kelly JB, Sally SL. Organization of auditory cortex in the albino rat: binaural response properties. *J Neurophysiol* 59: 1756–1769, 1988.

Kitzes L. Binaural interactions shape binaural response structures and frequency response functions in primary auditory cortex. *Hear Res* 238: 68–76, 2008.

Koka K, Read HL, Tollin DJ. The acoustical cues to sound location in the rat: measurements of directional transfer functions. *J Acoust Soc Am* 123: 4297–4309, 2008.

Kyweriga M, Stewart W, Wehr M. Neuronal interaural level difference response shifts are level-dependent in the rat auditory cortex. *J Neurophysiol* 111: 930–938, 2014.

Lee CC, Middlebrooks JC. Auditory cortex spatial sensitivity sharpens during task performance. *Nat Neurosci* 14: 108–114, 2011.

Li N, Gittelman JX, Pollak GD. Intracellular recordings reveal novel features of neurons that code interaural intensity disparities in the inferior colliculus. *J Neurosci* 30: 14573–14584, 2010.

Lu JP, Cui YL, Cai R, Mao YT, Zhang JP, Sun XD. Early auditory deprivation alters expression of NMDA receptor subunit NRI mRNA in the rat auditory cortex. *J Neurosci Res* 86: 1290–1296, 2008.

Markram H, Toledo-Rodriguez M, Wang Y, Gupta A, Silberberg G, Wu C. Interneurons of the neocortical inhibitory system. *Nat Rev Neurosci* 5: 793–807, 2004.

Miller LM, Escabi MA, Read HL, Schreiner CE. Functional convergence of response properties in the auditory thalamocortical system. *Neuron* 32: 151–160, 2001.

Ojima H, Murakami K. Intracellular characterization of suppressive responses in supragranular pyramidal neurons of cat primary auditory cortex in vivo. *Cereb Cortex* 12: 1079–1091, 2002.

Phillips DP, Irvine DR. Some features of binaural input to single neurons in physiologically defined area AI of cat cerebral cortex. *J Neurophysiol* 49: 383–395, 1983.

Polley DB, Read HL, Storace DA, Merzenich MM. Multiparametric auditory receptive field organization across five cortical fields in the albino rat. *J Neurophysiol* 97: 3621–3638, 2007.

Popescu MV, Polley DB. Monaural deprivation disrupts development of binaural selectivity in auditory midbrain and cortex. *Neuron* 65: 718–731, 2010.

Razak KA, Fuzessery ZM. GABA shapes a systematic map of binaural sensitivity in the auditory cortex. *J Neurophysiol* 104: 517–528, 2010.

Reid RC, Alonso JM. Specificity of monosynaptic connections from thalamus to visual cortex. *Nature* 378: 281–284, 1995.

Rutkowski RG, Wallace MN, Shackleton TM, Palmer AR. Organisation of binaural interactions in the primary and dorsocaudal fields of the guinea pig auditory cortex. *Hear Res* 145: 177–189, 2000.

Scholl B, Gao X, Wehr M. Nonoverlapping sets of synapses drive on responses and off responses in auditory cortex. *Neuron* 65: 412–421, 2010.

Sykova E. The extracellular space in the CNS: its regulation, volume and geometry in normal and pathological neuronal function. *Neuroscientist* 3: 28–41, 1997.

Tan AY, Atencio CA, Polley DB, Merzenich MM, Schreiner CE. Unbalanced synaptic inhibition can create intensity-tuned auditory cortex neurons. *Neuroscience* 146: 449–462, 2007.

Tan AY, Brown BD, Scholl B, Mohanty D, Priebe NJ. Orientation selectivity of synaptic input to neurons in mouse and cat primary visual cortex. *J Neurosci* 31: 12339–12350, 2011.

Thomson AM, Lamy C. Functional maps of neocortical local circuitry. *Front Neurosci* 1: 19–42, 2007.

Wehr M, Zador AM. Balanced inhibition underlies tuning and sharpens spike timing in auditory cortex. *Nature* 426: 442–446, 2003.

Wesolek CM, Koay G, Heffner RS, Heffner HE. Laboratory rats (*Rattus norvegicus*) do not use binaural phase differences to localize sound. *Hear Res* 265: 54–62, 2010.

Wilent WB, Contreras D. Dynamics of excitation and inhibition underlying stimulus selectivity in rat somatosensory cortex. *Nat Neurosci* 8: 1364–1370, 2005.

Williams SR, Mitchell SJ. Direct measurement of somatic voltage clamp errors in central neurons. *Nat Neurosci* 11: 790–798, 2008.

Wu GK, Li P, Tao HW, Zhang LI. Nonmonotonic synaptic excitation and imbalanced inhibition underlying cortical intensity tuning. *Neuron* 52: 705–715, 2006.

Wu GK, Tao HW, Zhang LI. From elementary synaptic circuits to information processing in primary auditory cortex. *Neurosci Biobehav Rev* 35: 2094–2104, 2011.

Xu F, Cai R, Xu JH, Zhang JP, Sun XD. Early music exposure modifies GluR2 protein expression in rat auditory cortex and anterior cingulate cortex. *Neurosci Lett* 420: 179–183, 2007.

Xu J, Yu L, Cai R, Zhang J, Sun X. Early continuous white noise exposure alters auditory spatial sensitivity and expression of GAD65 and GABAA receptor subunits in rat auditory cortex. *Cereb Cortex* 20: 804–812, 2010.

Yao JD, Bremen P, Middlebrooks JC. Rat primary auditory cortex is tuned exclusively to the contralateral hemifield. *J Neurophysiol* 110: 2140–2151, 2013.

Zhang J, Nakamoto KT, Kitzes LM. Binaural interaction revisited in the cat primary auditory cortex. *J Neurophysiol* 91: 101–117, 2004.

Zhang LI, Tan AY, Schreiner CE, Merzenich MM. Topography and synaptic shaping of direction selectivity in primary auditory cortex. *Nature* 424: 201–205, 2003.

Zhou Y, Liu BH, Wu GK, Kim YJ, Xiao Z, Tao HW, Zhang LI. Preceding inhibition silences layer 6 neurons in auditory cortex. *Neuron* 65: 706–717, 2010.